ORIGINAL PAPER

CrossMark

Tribological Characteristics of Aqueous Graphene Oxide, Graphitic Carbon Nitride, and Their Mixed Suspensions

Anshun He[1] · Shuiquan Huang[1] · Jung-Ho Yun[2] · Zhengyi Jiang[3] · Jason R. Stokes[2] · Sihai Jiao[4] · Lianzhou Wang[2] · Han Huang[1]

Abstract

The tribological performance of graphene oxide (GO), graphitic carbon nitride (g-C_3N_4), and their mixed (g-C_3N_4/GO) aqueous suspensions was investigated. The 0.06 wt% GO, 0.06 wt% g-C_3N_4, and 0.06 wt% 1:1 g-C_3N_4/GO suspensions reduced the coefficient of friction (COF) by 37, 26 and 37% and wear mark radius by 19.1, 16.0 and 19.6%, respectively, in comparison with water. Pure g-C_3N_4 and GO suspensions showed unstable lubrication in the tests with relatively high loads and speeds, while the g-C_3N_4/GO mixed suspension had superior tribological performance in all tested conditions. This is because in the mixed suspension g-C_3N_4 agglomerates became smaller, and GO nanosheets exhibited fewer wrinkles and less stacking, which enabled the formation of a layer of tribo-composite film. As a result, the friction, wear and tribo-corrosion were reduced during sliding.

Keywords Water-based lubricant · Tribology · Graphene oxide · Graphitic carbon nitride

1 Introduction

The use of oil-based lubricants in the manufacturing industry has raised environmental compatibility concerns. For a sustainable future, a great research effort has been focused on the development of environmentally friendly alternatives to replace oil-based lubricants [1]. Water-based lubricants have attracted great attention in academic and manufacturers because they are mostly environmental-friendly, highly flexible and thermal conductive [2]. Nevertheless, water itself cannot provide metallic contact systems with sufficient lubrication because of its low viscosity and poor lubricity. Previous studies [3–10] have demonstrated that the addition

of nanostructured materials, e.g. metal and metal oxide nanoparticles, carbon-based additives could improve the anti-frictional property of water-based solvents. However, such nanomaterials were prone to agglomeration because of their high surface-activity, which thus limited their anti-wear and friction-reduction effects. Although surfactants are likely to improve the colloidal stability of the nano-additive suspensions, it has been suggested that they would lead to issues including pollution, lubricating performance variation and high cost [11]. Therefore, the development of high-efficient additives with a good water-dispersing capacity is essential, but remains a bottleneck till now. Two-dimensional (2D) nanomaterials showed great potentials as the candidates for such applications.

Graphitic carbon nitride (g-C_3N_4) has received considerable attention as a novel 2D nanomaterial in numerous fields as it has good thermal and chemical stabilities and is readily dispersed in water [12, 13]. The layered structure of g-C_3N_4 with strong covalent bonds from C and N atoms and weak interlayer van der Waals force makes it an attractive nanomaterial for tribological applications [14]. However, till now, only the tribological performance of g-C_3N_4 in oil was reported [15]. As a typical 2D nanomaterial, graphene oxide (GO) has also received extensive attention in the field of tribology thanks to its one-atom thick layer structure and

✉ Han Huang
han.huang@uq.edu.au

[1] School of Mechanical and Mining Engineering, The University of Queensland, St Lucia, QLD 4072, Australia

[2] School of Chemical Engineering, The University of Queensland, St Lucia, QLD 4072, Australia

[3] School of Mechanical, Materials and Mechatronic Engineering, University of Wollongong, Wollongong, NSW 2522, Australia

[4] Research Institute (R&D Center), Baoshan Iron & Steel Co., Ltd., Shanghai 201900, China

weak van der Waals force in between adjacent layers, which allows low shearing strength for friction reduction [16]. It is also commonly known that GO can be readily dispersed in water by simple mechanical agitation methods due to its hydrophilic nature [17]. Several studies were concerned with the feasibility of GO used in water-based lubricants. For example, Song and Li [18] found that the GO nanofluid produced the significantly lower friction and wear in comparison with baseline water. Other studies also showed that the GO sheets could enter the contact area and provide lubricious effect due to its extremely thin laminated structure [19, 20]. Nevertheless, the tribological behaviour of aqueous GO suspension has not been systematically studied, and its lubricating mechanism is not well understood [21–23].

Recent studies showed that mixed suspensions that disperse solid nanosheets and nanoparticles with oil could enhance the tribological performance of the lubricants made of the respective constitutes owing to their synergic effect [24–26]. For example, Meng et al. [24] found that the friction and wear in the standardised four-ball tests were effectively reduced when using the lubricant that mixed nanosilver/graphene nanocomposites in engine oil. Xin et al. [26] demonstrated that GO/molybdenum disulphate (MoS_2) suspensions could reduce the friction and wear in a steel-on-steel sliding contact. Apparently, the tribological performance demonstrated by the mixed suspensions shows a great potential, yet their synergic lubricating mechanism needs further investigation.

In this study, the synthesis of an aqueous mixed lubricant that disperses g-C_3N_4 and GO nanosheets in water is reported. The friction and wear characteristics of such water-based lubricants were systematically studied under different tribological conditions, in comparison with case using pure water. The lubricating mechanisms of the mixed suspensions were discussed.

2 Experiments

2.1 Materials and Synthesis

The g-C_3N_4 nanosheets used in this study were synthesised using the method reported previously [27]. In the synthesis, dicyandiamide and ammonium chloride were mixed and processed to produce a pale yellow sponge-like material. The material was then dispersed under ultrasonication in deionised water. Upon completion, the obtained suspension was centrifuged and the sediment was removed. Eventually, fully exfoliated g-C_3N_4 nanosheets with a concentration of ca. 0.7 g/L were obtained. The morphology of the synthesised nanosheets was examined using a transmission electron microscopy (TEM, JEM 2100, JEOL, Japan) with an electron beam of 200 kV. The x-ray diffraction was

obtained using a Bruker D8 Advance powder XRD with a Cu radiation source of 40 kV. The grazing angle step was 0.2°, with 2θ ranged from 5° to 70°. X-ray Photoelectron Spectroscopy (XPS) was used to probe the chemical bonding of the synthesised materials. A mono Al Kα (1486.6 eV) x-ray source was used. PDF-4 + 2016 database was used for elemental analysis. Figure 1a shows the TEM image of a typical g-C_3N_4 agglomerate with porous sheet morphology. The nanosheets collapsed and intertwined to form a large irregular particle-like structure. The XRD spectrum shown in Fig. 1b presents two prominent peaks. The (100) peak at 13.1° corresponds to the in-plane structural packing of nitrogen-linked heptazine units with a lattice distance of 0.676 nm. The (002) peak at 27.5° is the signal from aromatic graphite lattices with an interplanar stacking distance of 0.324 nm. The g-C_3N_4 powder was obtained by drying the resultant suspension at 80 °C, and the XPS survey scan of the g-C_3N_4 nanosheets is shown in Fig. 1c. The two main components are nitrogen (399 eV) and carbon (532 eV), with the percentage of 55.93 and 42.49 at.%, respectively. The ratio of the content of these two components is 1.32, which is close to the atomic ratio of nitrogen to carbon of g-C_3N_4. As shown in Fig. 1d, the majority of carbon atoms are bonded to nitrogen, indicated by the large intensity of the peak at 280.0 eV, whereas a small amount of C–H and C–C bonds are presented. These results indicate the formation of exfoliated g-C_3N_4 nanosheets [12, 28, 29].

The GO nanosheets in powder form (analytical grade with a purity of > 97 wt%) were commercially available (supplied by Henqiu Graphene Tech. Co. Ltd, China). The as-received GO nanosheets have a lateral size varying from 10 to 50 μm and a thickness from 1 to 2 nm. Figure 1e shows the typical morphology of GO nanosheets with a large number of wrinkles or puckering in the lateral direction, which are the typical features of the unique one-layer structure. The XRD spectrum of GO nanosheets shown in Fig. 1f exhibits a dominant diffraction peak at 11.2°, which corresponds to (002) with an interlayer spacing of approximately 8.0 Å. This result shows a good agreement with that of typical GO nanosheets [4, 30, 31]. The minor peak at 20.9° indicates a smaller interlayer spacing of approximately 4.24 Å, possibly resulted from a small amount of stacking. Figure 1g shows the x-ray photoelectron spectroscopy (XPS) survey scan of the GO nanosheets. The two prominent peaks at 286 and 532 eV represent the two main components: carbon (67.96 at.%) and oxygen (32.06 at.%). The C1s spectra and the corresponding fitting curves of the GO sheets are shown in Fig. 1h, where C–C and C–O bonds are most prominent, reflected by the two major peaks at 284.6 and 286.5 eV, respectively. A few oxygen atoms are bonded to the carbon by double bonds and in the forms of carboxyl (COO) groups. These peaks indicated that for the GO nanosheets, carbon atoms form the
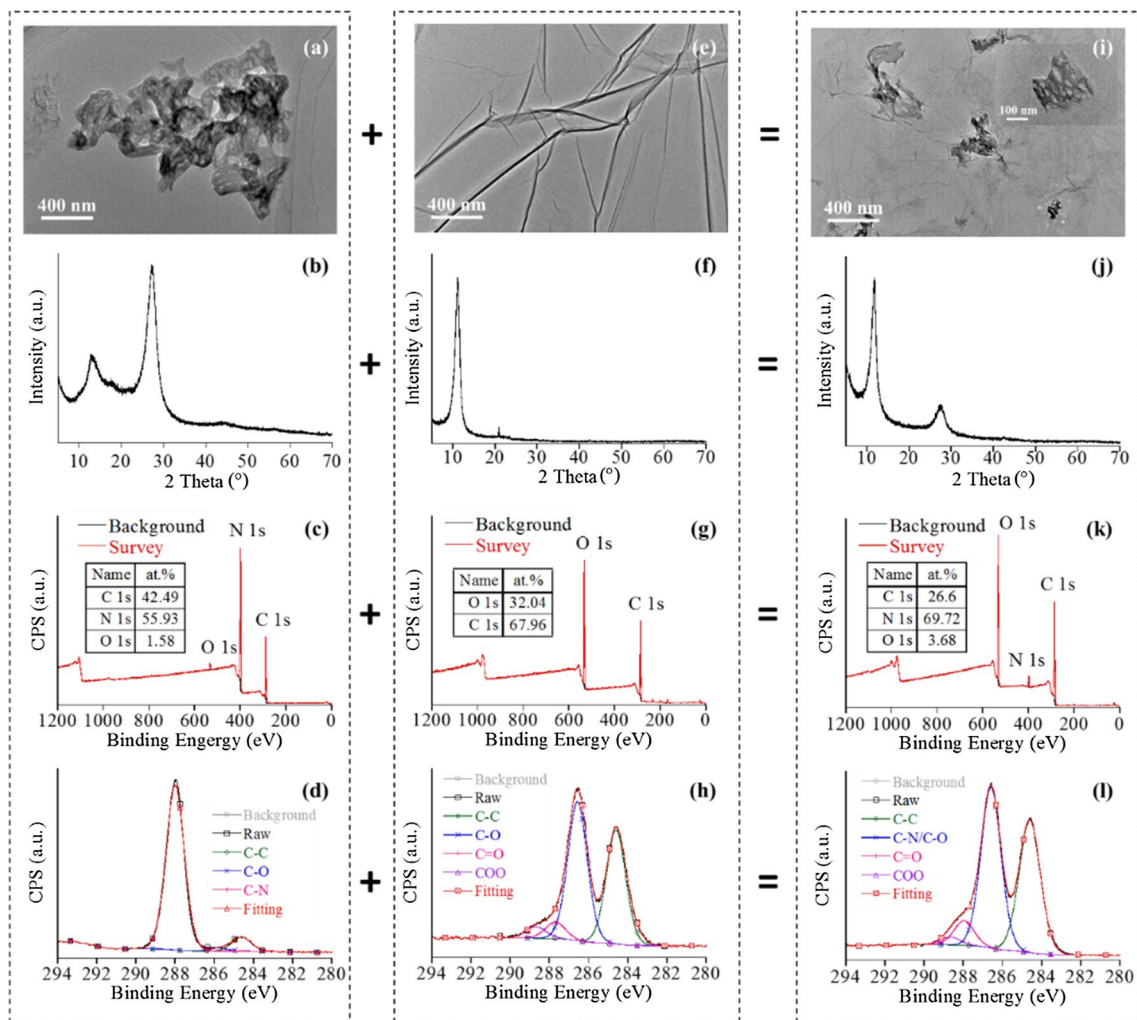
Fig. 1 TEM images, XRD spectra, XPS survey spectra and C1s spectra of **a–d** g-C_3N_4, **e–h** GO, and **i–l** g-C_3N_4/GO mixed suspensions

hexagonal backbone, while relatively smaller amount of oxygen atoms are bonded on the basal planes and edges of the sheets to form functional groups. These functional groups might bind to metal ions through both electrostatic interactions and coordination bonds to enhance contact affinity between GO sheets and steel surfaces [32].

To prepare g-C_3N_4/GO mixed suspension, the g-C_3N_4 and GO water-based suspensions were firstly prepared by a mechanical de-agglomeration process. In the process, 0.02, 0.04, 0.06, 0.08 and 0.1 wt% of g-C_3N_4 and GO powders were mixed in Milli-Q deionised water. g-C_3N_4 and GO suspensions were then mixed with the a weight ratio of 1:1. The concentration of a mixed suspension is defined as that of both g-C_3N_4 and GO to the suspension in this study. Subsequently, the g-C_3N_4/GO mixtures were stirred for 30 min, followed by ultrasonic bathing (Hwashin Tech. Co., Korea) for 15 min. The mixtures were further agitated by use of an ultrasonic probe (Branson Digital Sonifier 450, USA) at a power of 400 watts for 10 min with a 5-s on/off interval.

Circulated chilling water bath was used to maintain suspension temperature during the agitation process.

The prepared g-C_3N_4/GO mixed suspension was diluted by 50:1 and transferred to a copper grid for TEM observation. Figure 1i shows the typical mixed nanosheets, where normal wrinkles on the GO sheets shown in Fig. 1f became flattened, and the agglomerates of g-C_3N_4 were much smaller compared to that in Fig. 1a. The inset in Fig. 1i shows a typical g-C_3N_4 agglomerate anchored on a GO sheet. Figure 1j shows the XRD spectrum of g-C_3N_4/GO mixed nanosheets. The (002) peaks of GO and g-C_3N_4 are at 11.9° and 27.7°, respectively. The (100) heptazine characteristic peak of g-C_3N_4 overlaps the (002) peak, and the stacking peak of GO no longer exist. This indicated that the GO sheets might be fully exfoliated in the mixed suspension. As shown in Fig. 1k, the XPS survey scan of the g-C_3N_4/GO mixed nanosheets indicates that carbon and oxygen were the main components, with only small amount of nitrogen (3.68 at.%). The C1s spectra of g-C_3N_4/GO mixed nanosheets shown in Fig. 1l have similar components to that of

GO nanosheets. This is because the C–C and C-N bonds have very close characteristic binding energies, and therefore, they are difficult to separate from each other. The XPS results indicate that no new chemical bonds were created in the g-C_3N_4/GO mixed suspension.

2.2 Tribological Testing

Tribological performance of the water-based suspensions that use g-C_3N_4, GO and g-C_3N_4/GO nanosheets as additives was investigated on a Modular Compart Rheometer (or MCR-502, Anton Paar, Austria) with a tribological ball-on-three-plate testing configuration. Grade 10 (Ra = 23.2 ± 2.5 nm) AISI 52100 Cr alloy steel and polished (Ra = 37.0 ± 6.2 nm) AISI 304 stainless steel were used as the ball and plate materials, respectively. During a tribological test, the ball is vertically pressed on three plates, which are fixed at 45° about the loading axis. The normal load used in this study was ranged from 10 to 35 N, corresponding to a Hertzian contact pressure of 645 to 981 MPa. The sliding speed varied from 25 to 125 mm/s. For comparable wear mark analysis, the total sliding distance was maintained at 7.5 m. The sliding distance was set as such so that the run-in periods of the sliding can be completed to obtain a stable COF, which will be further discussed in the later sections. Prior to testing, all components were washed in acetone using a sonication bath. The contact areas were completely submerged in the tested lubricants. During testing, the temperature of the contact pair was maintained at 25 °C using a built-in chilling water circulation system. New balls and plates were used for every test to ensure repeatability. At least three tests were performed for every condition.

2.3 Characterisation of Wear Marks

The plates after tribological testing were collected for wear mark size measurement and surface analysis. The plates were agitated in an ultrasonic bath for 10 min to remove any loose debris and residues of lubricants prior to examination. A confocal microscope (LEXT OLS4100, Olympus, Japan) was used to examine the wear marks. The wear marks were also examined using a scanning electron microscope (JEOL JSM-6610, Japan). A working energy of 20 kV was used with a working distance of 10 mm. Elemental analysis of the wear marks was performed on a Renishaw Raman microscope with a 514 nm laser beam.

3 Results and Discussion

3.1 Optimal Concentration

The effect of concentration of the g-C_3N_4, GO and mixed suspensions on the COF and wear mark radius is shown in

Fig. 2. It is noted that the mixed suspensions being studied had a g-C_3N_4/GO ratio of 1:1, so its concentrations shown in Fig. 2 represent the values of both g-C_3N_4 and GO. For comparison, the COF and wear mark radius with water is also plotted (referred to by the concentration of 0 wt%).

It is seen from Fig. 2a that when the concentration of the nanosheets increased, the COF decreased. For the g-C_3N_4 suspension (red line), the addition of 0.02 wt% reduced the COF from 0.4 (for water) to 0.3, about the reduction in 21%, compared with that of the baseline water. But the COF remained almost unchanged with further increase in concentration. For the GO suspensions, the COF gradually decreased to 0.21 as the concentration increased to 0.1 wt%, corresponding to the reduction in 46%, in comparison with water. For the g-C_3N_4/GO mixed suspension, the COF also decreased with the increased concentration, showing a reduction in 42% at the greatest concentration of 0.1 wt%.

Figure 2b shows the effect of concentration on wear mark radius. For all the three suspensions, the wear mark radius decreased with the increased concentration, reached the minimum radius at the concentration of 0.06 wt%, and then increased with the further increase in concentration. The maximum reductions in wear mark radius were 16.0, 19.1, and 19.6% for g-C_3N_4, GO and g-C_3N_4/GO mixed suspensions, respectively, compared to that of water. When the concentration was relatively low, an effective tribo-thin film could not be formed because insufficient nanosheets could get into the contact area. As the concentration increased,
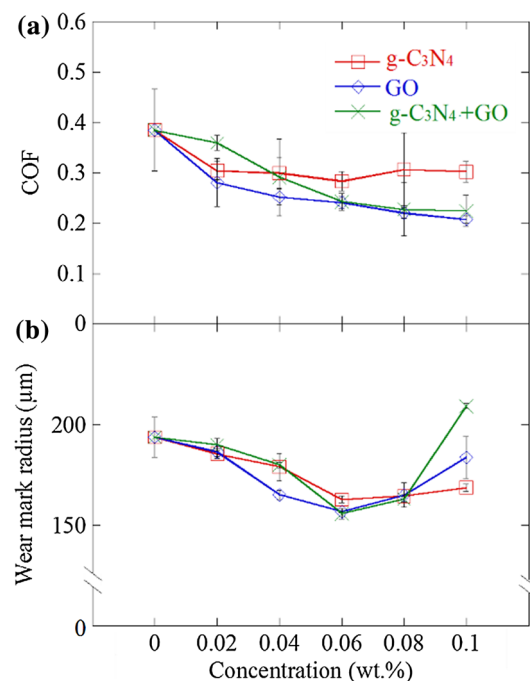

Fig. 2 The effects of concentration on **a** COF and **b** wear mark radius using g-C_3N_4, GO and g-C_3N_4/GO mixed suspensions

Table 1 Reductions in COF and wear mark radius of the nano-additive water lubricants, in comparison with water

Lubricant	COF	Reduction (%)	Wear mark radius (µm)	Reduction (%)
Water	0.38	N/A	194	N/A
0.06 wt% GO	0.24	37	157	19.1
0.06 wt% g-C_3N_4	0.28	26	163	16.0
0.06 wt% g-C_3N_4/GO	0.24	37	156	19.6
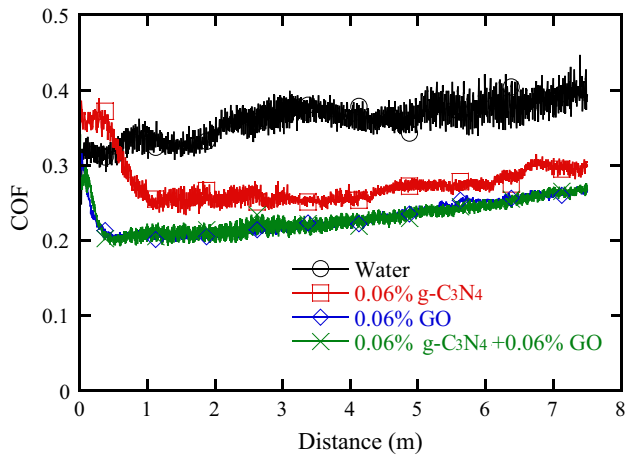
Fig. 3 The values of COF plotted as a function of sliding distance for three different aqueous suspensions. Water serves as a benchmark (Color figure online)

both COF and wear were reduced. However, excessive nanosheets could result in unstable dispersion and relatively large agglomerates, which in turn caused increase in wear [2].

Based on the tribological performance shown in Fig. 2, 0.06 wt% was selected as the optimal concentration to make nanosheet suspensions. The reduction in the values of COF and wear mark radius resulted from the use of the optimal concentration of GO, g-C_3N_4 and g-C_3N_4/GO suspensions are summarised in Table 1, in comparison with those from

water. The concentration thus remained unchanged in the further study.

3.2 Tribological Characteristics

Figure 3 shows the COF plotted as a function of sliding distance during the tribological tests using water, 0.06 wt% GO, 0.06 wt% g-C_3N_4 and 0.06 wt% 1:1 g-C_3N_4/GO mixed suspensions. With water as lubricants, the COF started at 0.34 and continued to increase to 0.40 over the total testing distance. The COF values exhibit relatively large fluctuation (approximately 16% of the average COF), likely due to the contact vibration and noise caused by insufficient lubrication. When the three synthesised suspensions were used, the fluctuation in their COF curves (red, blue and green curves) was significantly reduced. Also, different from water, the values of COF for all nanosuspensions decreased by approximately 30% at the early stage of sliding (~ 1 m), which is well known as the run-in period [33, 34]. In this period, the contact area size increased rapidly to a stable value via asperity contact wear. As the run-in period is not stable, in this study, the average COF was calculated using the values collected after the run-in period.

The wear marks on the plates after the tribological tests with different lubricating conditions are shown in Fig. 4. The arrow in the figure shows the sliding direction from left to right for all images. As shown in Fig. 4a, the wear mark being generated with water as lubricants is slightly larger compared to those using synthesised suspensions shown in Fig. 4b–d. The surface in Fig. 4a is reflective, scattered with corrosion marks and long scratches, which are typical signs of adhesion wear and tribo-corrosion caused by water [10]. On the entry side of the wear mark, there exists a dark mark, which is most likely attributed to the accumulation of oxide debris carried into the contact by the water flow during sliding. Those oxide debris is harder than steel and would act as abrasives to scratch the steel plate. The accumulated oxide at the entry side would also cause starvation of water. The combining effects of adhesive and abrasive wear thus resulted in large wear mark, as well as noise and vibration
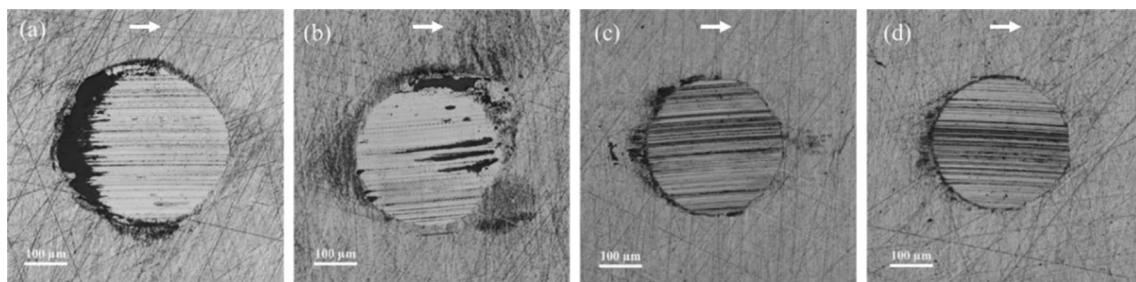
Fig. 4 Confocal microscope images of the wear marks obtained using **a** water, **b** 0.06 wt% g-C_3N_4, **c** 0.06 wt% GO, and **d** 0.06 wt% g-C_3N_4/GO mixed suspensions with the normal load of 20 N and sliding speed of 50 mm/s

that was reflected in the highly fluctuated COF curves shown in Fig. 3 (black curve).

The wear mark produced by using the 0.06 wt% g-C$_3$N$_4$ suspension is covered with broken-dot-patterned scratches, as shown in Fig. 4b. There also exist some dark marks, similar to but smaller than that in Fig. 4a. This might be because g-C$_3$N$_4$ nanosheets entered the contact area and created separation, but also allowed the oxide debris generated by tribo-corrosion to get entrained into the contact. The hard iron oxide would scratch the plate surface. However, in this case, oxide accumulation was not found on the entry side. This means that constant replenishment of fresh g-C$_3$N$_4$ suspension was maintained during sliding. Therefore, the friction is lower than that using water with smaller fluctuation.

The wear mark produced by using the 0.06% GO suspension is shown in Fig. 4c. The worn surface is covered with obvious scratches along the sliding direction, but is free of accumulation of debris, which is different from those shown in Fig. 4a, b. This is because tribo-corrosion was relieved, likely due to the protective effect of GO sheets on the rubbing surfaces. The scratches on the worn surface should be attributed to the abrasive wear by the small sized GO sheets with relatively high estimated hardness [35], which may be imbedded in the contact rather than adhering to the surface. Similar scratches induced by small sized GO sheets were reported [36, 37].

Figure 4d shows the wear mark being generated by the mixed suspension. The worn surface is free of iron debris, and more scratches can be seen at the centre of the mark than the sides. The worn surface characteristics suggest that tribo-corrosion was effectively suppressed, most likely due to the protection of the tribo-thin film formed by the nanosheets. As the g-C$_3$N$_4$ sheets are thicker than the GO sheets, it is thus derived that the g-C$_3$N$_4$ sheets might have protected the surrounding area of the contact, while the thinner GO nanosheets could enter the centre area to take the role of a lubricant. The roles of g-C$_3$N$_4$ and GO nanosheets in the mixed suspension will be further discussed in the following sections.

3.3 Effect of Testing Load

Figure 5 shows the effect of load on the COF and wear radius obtained from the tribological tests performed at the constant sliding speed of 50 mm/s using water, and nanosheet concentration of 0.06 wt% g-C$_3$N$_4$, GO and g-C$_3$N$_4$/GO mixed suspensions as lubricants, respectively. When water was used, the COF remained at a high value of 0.37 ± 0.08 in the load range of 10 to 25 N. At 30 N, the COF increased to 0.51 ± 0.11. The large error bars in the COF also indicate the unstable sliding with water. In comparison, with the synthesised suspensions, the error bars are much smaller than those for water, indicating a much smoother sliding during
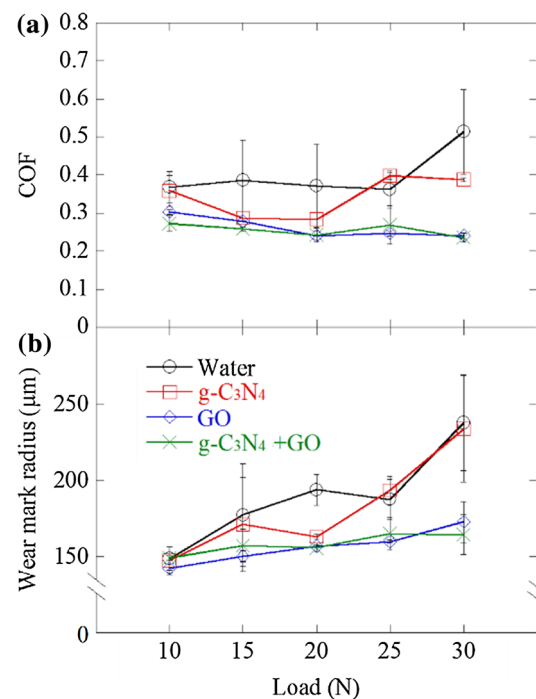

Fig. 5 The effect of load to the **a** COF and **b** wear mark radius obtained using 0.06 wt% g-C$_3$N$_4$, 0.06 wt% GO and 0.06 wt% g-C$_3$N$_4$/GO (1:1) suspensions. Water serves as a benchmark

the test. For the g-C$_3$N$_4$ suspension, the COF dropped to 0.30 when the load was increased from 10 to 20 N, but the COF increased with further increase in load. The effect of load on COF values was insignificant when using GO and g-C$_3$N$_4$/GO mixed suspensions as lubricants, with their average COF values slightly decreased with the increased load. Figure 5b shows the effect of load on wear. In general, when water and g-C$_3$N$_4$ suspension were used as lubricants, the resultant wear mark radius increased significantly by 60% with the increase in normal load from 10 to 30 N. This result is consistent with the well-reported observation of the tribological behaviour of water, where the increase in contact pressure enhanced friction [38]. When GO and g-C$_3$N$_4$/GO mixed suspensions were used, much smaller wear marks were observed for all tested loads. When the load increased from 10 to 30 N, the increase was only 21% and 10%, for GO and g-C$_3$N$_4$/GO mixed suspensions, respectively.

3.4 Effect of Sliding Speed

Figure 6a shows the effect of sliding speed ranging on the COF from the tribological tests using water, g-C$_3$N$_4$, GO, and g-C$_3$N$_4$/GO suspensions as lubricants. With water, as the sliding speed increased, the COF was reduced from 0.56 ± 0.15 at 25 mm/s to 0.32 ± 0.07 at 75 mm/s and remained almost unchanged when the sliding speed was further increased. When the g-C$_3$N$_4$ suspension was applied,

the COF showed a similar trend to that of water, which decreased from 0.53 ± 0.06 at 25 mm/s to 0.28 ± 0.02 at 50 mm/s, but slightly increased to 0.36 ± 0.05 when the speed was further increased to 125 mm/s. When GO suspension was used, the COF was stable at approximately 0.25 ± 0.03 from 25 to 100 mm/s, and then the value started to climb to 0.32 ± 0.03 at 125 mm/s. For the g-C_3N_4/GO mixed suspension, the COF was not significantly affected by the change of sliding speed, being at approximately 0.25 for the whole tested range.

Figure 6b shows the wear mark radius obtained from the tests. When using water as lubricants, the wear mark radius decreased from 206 μm at 25 mm/s to 165 μm at 75 mm/s, and remained at the same level with further increase in sliding speed. The reduction in wear is because the hydrodynamic lubrication was more prevailing, which increased the separation of contact due to the increase in sliding speed. This result agrees well with that reported previously [39]. For the g-C_3N_4 suspension, the wear mark radius decreased from 214 to 163 μm from 25 to 50 mm/s. When the speed was further increased, the wear mark remained at the same value at about 165 μm. The wear mark radius of the GO suspension showed a different trend compared to those of other suspensions. At low speeds of 25 and 50 mm/s, the radius was about 170 μm, but increased significantly to 295 μm when the speed increased to 75 mm/s and above. When g-C_3N_4/GO mixed suspension was applied, the wear
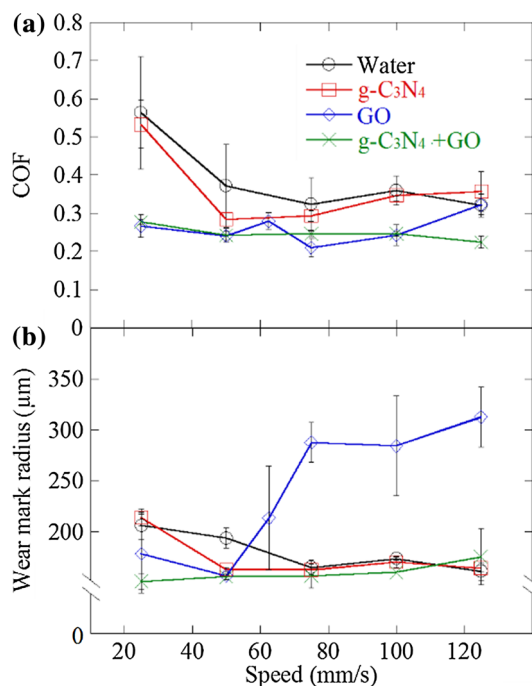
mark radius was stable at the lowest level of about 158 μm for the entire tested range. The effect of lubrication mode change is insignificant because the mixed g-C_3N_4/GO structure played a predominant role in the contact area within the whole speed range.

3.5 Wear Mark Characteristics

Figure 7 shows the backscattered electron SEM images (left) and the corresponding Raman spectra (right) of the dark and light scratches on the wear marks after the tribological tests using g-C_3N_4, GO and g-C_3N_4/GO suspensions as lubricants under different loads and speeds. As shown in Fig. 7a, when the applied load was 20 N using g-C_3N_4 suspension, wide dark scratches were observed, likely due to the coupling effect of contact vibration and work hardening [10]. The Raman spectra of the reference area (or non-contact area) and light scratches showed no detectable signal, while for the dark scratches, a strong band at 699 cm^{-1} was observed, which belongs to Fe_3O_4 [40]. This indicates a high content of Fe_3O_4 on the wear mark surface.

When the load was increased to 25 N, as shown in Fig. 7b, the surface was smoother than that (at 20 N) in Fig. 7a with some scattered scratches. Again, no detectable signal was found from the Raman spectra of the reference area and light scratches. However, the Raman band of Fe_3O_4 became weaker. This indicates that the Fe_3O_4 debris being generated from oxidation could not enter the contact because the increased contact pressure reduced the separation space created by the lubricants. As mentioned earlier, the debris might accumulate at the entry side and cause starvation of lubrication in the contact area. Under such circumstance, the COF and wear mark radius would increase to the same level as those for water with the increased load.

At the sliding speed of 50 mm/s, using GO suspension as the lubricant produced wear mark surfaces with straight and narrow scratches, and the Raman spectra on the same wear surface exhibit no the iron oxide peaks, as shown in Fig. 7c. Two significant bands at 1360 and 1595 cm^{-1} that represent the D and G bands of GO, respectively, were observed on the dark scratches (see the blue curve), but the intensities of these two bands were much smaller on the spectrum of light scratches (see the green curve). The ratio of the intensities of these two bands (I_D/I_G) reflects the number of defects and degree of functionalisation on the nanosheets [2, 41]. At this speed, the residual GO sheets have an I_D/I_G of 0.90. These results clearly suggest that a weak layer of GO tribo-thin film might be formed during sliding, which thus reduced friction and wear. Some GO sheets of small lateral sizes imbedded on the substrate could still scratch the contact surface. The increase in sliding speed to 75 mm/s resulted in different wear mark morphology, as shown in Fig. 7d,
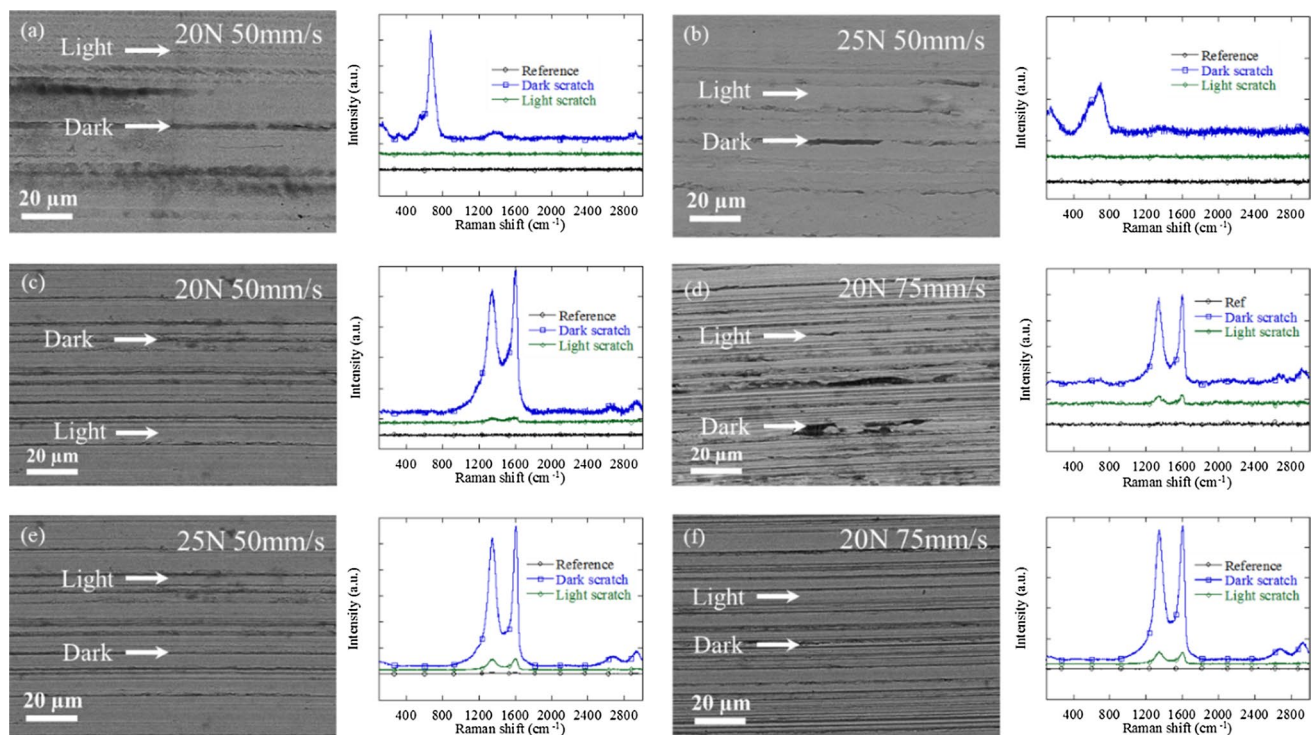

Fig. 6 The effect of sliding speed to the **a** COF and **b** wear mark radius obtained using 0.06 wt% g-C_3N_4, 0.06 wt% GO and 0.06 wt% g-C_3N_4/GO (1:1) suspensions. Water serves as a benchmark

Fig. 7 Backscattered SEM images (left) with corresponding Raman spectra (right) of the worn surfaces after the tribological tests using g-C$_3$N$_4$ (**a**, **b**), GO (**c**, **d**) and g-C$_3$N$_4$/GO (**e**, **f**) suspensions at various loads and speed as indicated

where the scratches were noticeably denser, some are wider, and irregular fracturing spots could be observed. Similar Raman spectrum of GO residues to that shown in Fig. 7c was obtained, but the I_D/I_G ratio was 0.95, slightly greater than that at 50 mm/s. This indicates that more defects were introduced to the GO sheets at higher speed.

Figure 7e shows the wear mark surface when using the g-C$_3$N$_4$/GO mixed suspension at the load of 25 N, whose surface is covered with fine and narrow scratches. The Raman spectra of the dark and light scratches both exhibit obvious D and G bands. The I_D/I_G is approximately 0.92, showing low level of defects. Apparently, the mixed suspension that consists of g-C$_3$N$_4$ anchored on the GO sheets (see Fig. 1i) would increase the separation between the contact pair, which in turn promoted the penetration of GO sheets into the contact area during sliding. When the sliding speed was increased, such as the case of 75 mm/s as shown in Fig. 7f, the density of scratches slightly increased compared to that obtained from the lower speed. In this case, the Raman spectra are similar to those at lower speed in Fig. 7e. With the mixed suspensions, fracturing spots found on the wear marks using the GO suspension shown in Fig. 7d disappeared.

3.6 Used Lubricant Characteristics

Figure 8a, b shows the TEM images of the used g-C$_3$N$_4$ suspensions after the tribological test using a load of 20 N and a sliding speed of 50 mm/s. Relatively large aggregation and intertwining of g-C$_3$N$_4$ nanosheets can be observed in the figures, and nanosheets appeared being folded up at the edges into tentacle-like structures. Figure 8c, d shows the used g-C$_3$N$_4$ suspension tested at a higher load of 25 N. The agglomerates are even larger than those in Fig. 8a, but the edges of the g-C$_3$N$_4$ nanosheets are not folded, indicating that the nanosheet might not enter the contact area during testing.

Figure 8e, f shows the GO sheets after the test at a load of 20 N and a sliding speed of 50 mm/s. The used nanosheets remained their intact laminar morphology. Black dots were found to be scattered on the sheets, which are likely the wear debris. When the sliding speed was increased to 75 mm/s, the used GO nanosheets are noticeably different from those from the test with a lower sliding speed, as shown in Fig. 8g, h. More wrinkles with deeper contrast appeared on the nanosheets. Also, sharp lateral cracks could be found at the end of wrinkles. This result agrees well with that derived
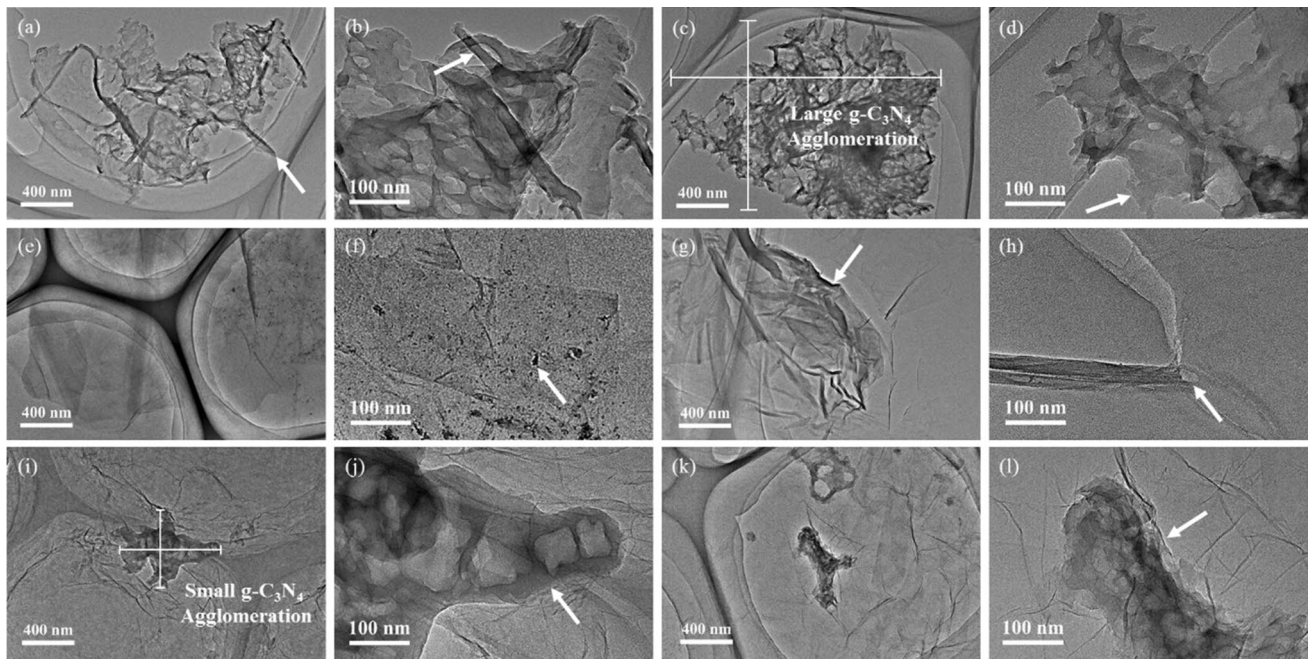
Fig. 8 TEM images of used g-C_3N_4 suspensions tested at **a**, **b** 20 N and 50 mm/s; **c**, **d** 25 N and 50 mm/s; GO suspensions tested at **e**, **f** 20 N and 50 mm/s, **g**, **h** 20 N and 75 mm/s; g-C_3N_4/GO suspensions used at **i**, **j** 25 N and 50 mm/s, **k**, **l** 20 N and 75 mm/s

from the Raman spectra shown in Fig. 7c, d, where the increased defects were found at a higher sliding speed.

Figure 8i, j shows the g-C_3N_4/GO mixed suspension after testing with a load of 25 N and a sliding speed of 50 mm/s. Compared to the test with the g-C_3N_4 suspension shown in Fig. 8c, d, the g-C_3N_4 agglomerates are significantly smaller and have smoother edges. The addition of GO sheets effectively reduced the tendency of agglomeration of g-C_3N_4 and protected the g-C_3N_4 from folding-up. Figure 8k, l shows the used g-C_3N_4/GO mixed suspension after the test at a higher speed of 75 mm/s. A similar wear morphology to the previous case (Fig. 8i) can be seen, where the g-C_3N_4 sheets remained intact. The large wrinkles and cracks observed in Fig. 8g, h could not be found, indicating that the imbedding of g-C_3N_4 on GO sheets would be beneficial to the prevention of GO nanosheets from being winkled.

3.7 Lubrication Mechanism

Based on the analysis above, the lubrication mechanism of the water-soluble carbon-based 2D suspensions can be summarised. The schematics of the sliding contact using nanosheets and mixed suspensions as lubricants in comparison with that of water are shown in Fig. 9.

With water, the friction is dominated by direct asperity contact, as illustrated in Fig. 9a. It is well documented [38] that due to the great pressure induced at the contact area, adhesive wear via plastic deformation might occur. Microwelding and re-breaking of the contact pairs could cause

severe vibration and thus significant friction force, which was evidenced by the high COF value and large fluctuations, as shown in Fig. 3. The elevated temperature in localised area due to the increased friction would enhance tribo-corrosion, leading to the formation of debris containing Fe_3O_4. Some of iron oxide debris were carried away by the water flow, but some were accumulated on the entry site of the contact, as shown in Fig. 4a. The accumulation could cause starvation of water in the contact, and in turn, resulted in further rise of localised temperature. When debris entered the contact area, abrasive wear occurred and scratches were generated, because the oxides had much higher hardness than that of the substrate steel.

In the g-C_3N_4 suspension, intertwined g-C_3N_4 nanosheets agglomerated and separated the contact pair, as shown in Fig. 9b. In some regions, asperity contact and tribo-corrosion still took place because of the uneven distribution of the nanosheets. Nevertheless, the lubrication was substantially improved, compared to that using water, and the oxide debris no longer accumulated on the entry side of the contact, as can be seen from the wear mark shown in Fig. 4. The separation space between the ball and the plate would decrease with the increased load. When the applied load was sufficiently high, g-C_3N_4 nanosheets might not be able to enter the contact area at all. This is why the g-C_3N_4 suspensions produced similar values of COF and wear mark radius to the respective values obtained from using water at high loads, as can be seen in Fig. 5, as well as the morphology shown in Fig. 8c, d.
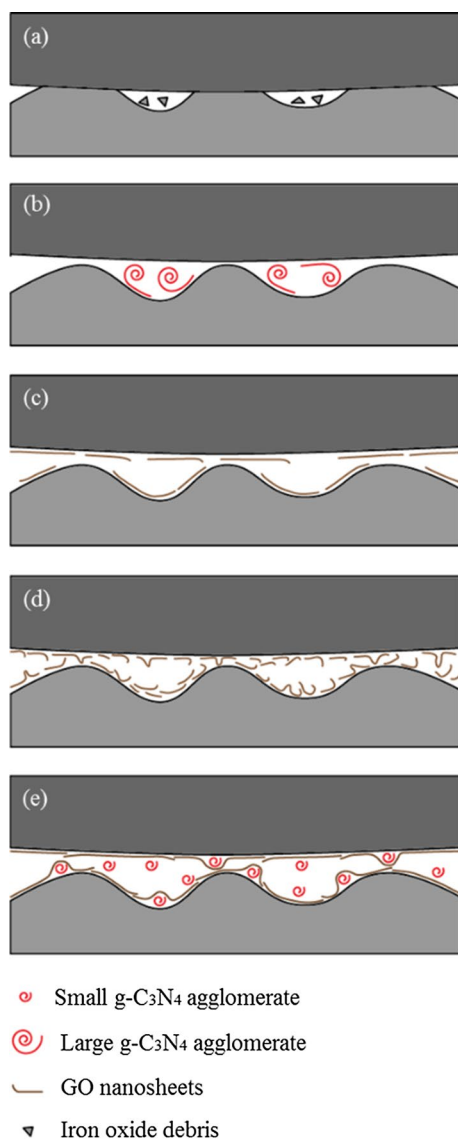
Fig. 9 Schematic illustrations of the contacts using **a** water, **b** g-C₃N₄ suspension, **c** GO suspension at 50 mm/s, **d** GO suspension at 75 mm/s, and **e** g-C₃N₄/GO mixed suspension as lubricants

Figure 9c shows the normal contact scenario when GO suspension was used as the lubricant at relatively low sliding speeds. GO nanosheets could effectively cover the surfaces of contact pairs because of their high affinity to the steel surfaces [2, 36]. As a result, direct asperity contact was effectively reduced, and the steel substrate was prevented from tribo-corrosion. As GO sheets have relatively low shear strength along their lateral orientation, interlayer sliding was easy and smooth with no vibration, which is reflected by the low and stable COF values being produced, as shown in Fig. 3. At relatively high sliding speeds, GO nanosheets were puckered and torn down probably due to the lack of replenishing sheets at high speed. The broken GO sheets became stronger due to size reduction and thus made

dense scratches similar to third-body abrasives, as shown in Fig. 9d. Such third-body abrasives also caused an unstable tribological performance, resulted in the large wear mark radius and increased COF.

Figure 9e schematically shows how the g-C₃N₄/GO mixed suspension works in the contact area during sliding. In the mixed suspension, g-C₃N₄ nanosheets were uniformly imbedded onto GO nanosheets to form a composite structure, as can be seen in Fig. 1i. Once the mixed nanosheets entered the contact area, the GO nanosheets would cover contact pairs to prevent them from tribo-corrosion and reduce friction, while the g-C₃N₄ nanosheets helped maintain the separation to make sure sufficient suspension enter the contact zone. The mixed structure ensured that lubricants could enter the contact area even under high speeds or high loads. Such a structure would also benefit to the reduction in puckering and stacking of GO sheets, leading to less abrasive wear. Similar synergic structures were reported previously [23].

4 Conclusions

The GO and g-C₃N₄ nanosheets and their mixed water suspensions were synthesised, and their tribological properties were investigated using a ball-on-three-plate tribometer with a steel-on-steel contact. The optimal concentrations for GO and g-C₃N₄ suspensions are both 0.06 wt% and those for g-C₃N₄/GO suspensions were 0.06 wt% at the ratio of 1:1, in terms of tribological performance. The use of GO and g-C₃N₄ nanosheets and their mixed suspensions could reduce the COF up to 37, 26 and 37% (i.e. 0.24, 0.28 and 0.24) and the wear mark radius up to 19.1, 16.0 and 19.6% (i.e. 157, 162 and 156 μm), respectively, in comparison with water. The g-C₃N₄/GO mixed suspensions showed superior tribological performance for all testing conditions, especially performed much better than GO or g-C₃N₄ suspension under the testing conditions of relatively high loads and speeds.

The lubrication mechanisms of the GO, g-C₃N₄ and g-C₃N₄/GO mixed suspensions were revealed in comparison with water. With water as lubricants, welding and breaking of asperities took place due to the large localised contact pressure, and oxide debris generated from tribo-corrosion accumulated at the entry side of the contact, and severe scratches were created on the contact surface. Using GO suspensions, tribo-corrosion could be effectively suppressed due to the coverage of tribo-thin film formed by GO nanosheets at relatively low sliding speeds. However, at relatively high sliding speeds, the GO tribo-film did not work effectively and abrasive wear could still be induced by sharp edges of GO sheets. The g-C₃N₄ nanosheets could separate the contact pair and thus reduce friction, but at relatively high loads, the g-C₃N₄ agglomerates could not efficiently

enter the contact area due to its squeezed separation space. The mixing of g-C_3N_4 and GO nanosheets produced a composite material with g-C_3N_4 agglomerates imbedded into GO nanosheets, leading to smaller g-C_3N_4 agglomerates and GO nanosheets with fewer wrinkles and stacking in the water suspension. The mixed suspension could thus easily form tribo-thin film to reduce friction, lower wear and prevent the contact pair from tribo-corrosion. The tribological performance of the mixed suspension was especially superior when testing at relatively high loads or speeds due to its unique composite structure.

References

1. Bartz, W.J.: Lubricants and the environment. Tribol. Int. **31**(1–3), 35–47 (1998)
2. Liang, S., Shen, Z., Yi, M., Liu, L., Zhang, X., Ma, S.: In-situ exfoliated graphene for high-performance water-based lubricants. Carbon **96**, 1181–1190 (2016)
3. Liang, S.S., Shen, Z.G., Yi, M., Liu, L., Cai, C.J., Zhang, X.J., et al.: Stable aqueous dispersion of exfoliated graphene for tribological applications. J. Nanosci. Nanotechno. **16**(2), 1491–1497 (2016)
4. Elomaa, O., Singh, V.K., Iyer, A., Hakala, T.J., Koskinen, J.: Graphene oxide in water lubrication on diamond-like carbon vs. stainless steel high-load contacts. Diam. Relat. Mater. **52**, 43–48 (2015)
5. Gu, Y., Zhao, X.C., Liu, Y., Lv, Y.X.: Preparation and tribological properties of dual-coated TiO_2 nanoparticles as water-based lubricant additives. J. Nanomater. **2014**, 1–8 (2014)
6. Zhao, C.L., Chen, Y.K., Ren, G.: A study of tribological properties of water-based ceria nanofluids. Tribol. Trans. **56**(2), 275–283 (2013)
7. Liu, Y.H., Wang, X.K., Pan, G.S., Luo, J.B.: A comparative study between graphene oxide and diamond nanoparticles as water-based lubricating additives. Sci. China Technol. Sc. **56**(1), 152–157 (2013)
8. Cho, D.H., Kim, J.S., Kwon, S.H., Lee, C., Lee, Y.Z.: Evaluation of hexagonal boron nitride nano-sheets as a lubricant additive in water. Wear **302**(1–2), 981–986 (2013)
9. Zhang, L.L., Pu, J.B., Wang, L.P., Xue, Q.J.: Frictional dependence of graphene and carbon nanotube in diamond-like carbon/ionic liquids hybrid films in vacuum. Carbon **80**, 734–745 (2014)
10. He, A., Huang, S., Yun, J.-H., Wu, H., Jiang, Z., Stokes, J., et al.: Tribological performance and lubrication mechanism of alumina nanoparticle water-based suspensions in ball-on-three-plate testing. Tribol. Lett. **65**(2), 40 (2017)
11. Sulek, M.W., Wasilewski, T.: Tribological properties of aqueous solutions of alkyl polyglucosides. Wear **260**(1), 193–204 (2006)
12. Wang, Y., Wang, X., Antonietti, M.: Polymeric graphitic carbon nitride as a heterogeneous organocatalyst: from photochemistry to multipurpose catalysis to sustainable chemistry. Angew. Chem. Int. Edit. **51**(1), 68–89 (2012)
13. Goettmann, F., Fischer, A., Antonietti, M., Thomas, A.: Metal-free catalysis of sustainable Friedel–Crafts reactions: direct activation of benzene by carbon nitrides to avoid the use of metal chlorides and halogenated compounds. Chem. Commun. **43**, 4530–4532 (2006)
14. Adachi, K., Kato, K.: Tribology of carbon nitride coatings, pp. 339–361. Springer, Berlin (2008)
15. Liu, X.X., Yamaguchi, R., Umehara, N., Deng, X.R., Kousaka, H., Murashima, M.: Clarification of high wear resistance mechanism of ta-CNx coating under poly alpha-olefin (PAO) lubrication. Tribol. Int. **105**, 193–200 (2017)
16. Spear, J.C., Ewers, B.W., Batteas, J.D.: 2D-nanomaterials for controlling friction and wear at interfaces. Nano Today **10**(3), 301–314 (2015)
17. Berman, D., Erdemir, A., Sumant, A.V.: Graphene: a new emerging lubricant. Mater. Today **17**(1), 31–42 (2014)
18. Song, H.J., Li, N.: Frictional behavior of oxide graphene nanosheets as water-base lubricant additive. Appl. Phys. A Mater. **105**(4), 827–832 (2011)
19. Rasheed, A.K., Khalid, M., Rashmi, W., Gupta, T.C.S.M., Chan, A.: Graphene based nanofluids and nanolubricants—review of recent developments. Renew. Sust. Energy Rev. **63**, 346–362 (2016)
20. Kinoshita, H., Nishina, Y., Alias, A.A., Fujii, M.: Tribological properties of monolayer graphene oxide sheets as water-based lubricant additives. Carbon **66**, 720–723 (2014)
21. Zhou, Q., Huang, J.X., Wang, J.Q., Yang, Z.G., Liu, S., Wang, Z.F., et al.: Preparation of a reduced graphene oxide/zirconia nanocomposite and its application as a novel lubricant oil additive. RSC Adv. **5**(111), 91802–91812 (2015)
22. Meng, Y., Su, F.H., Chen, Y.Z.: Synthesis of nano-Cu/graphene oxide composites by supercritical CO_2-assisted deposition as a novel material for reducing friction and wear. Chem. Eng. J. **281**, 11–19 (2015)
23. Meng, Y., Su, F.H., Chen, Y.Z.: A novel nanomaterial of graphene oxide dotted with Ni nanoparticles produced by supercritical CO_2-assisted deposition for reducing friction and wear. ACS Appl. Mater. Interfaces **7**(21), 11604–11612 (2015)
24. Meng, Y., Su, F., Chen, Y.: Supercritical fluid synthesis and tribological applications of silver nanoparticle-decorated graphene in engine oil nanofluid. Sci. Rep. **6**, 31246 (2016)
25. Shao, W., Liu, X., Min, H., Dong, G., Feng, Q., Zuo, S.: Preparation, characterization, and antibacterial activity of silver nanoparticle-decorated graphene oxide nanocomposite. ACS Appl. Mater. Interfaces **7**(12), 6966–6973 (2015)
26. Xin, Y., Li, T., Gong, D., Xu, F., Wang, M.: Preparation and tribological properties of graphene oxide/nano-MoS_2 hybrid as multidimensional assembly used in the polyimide nanocomposites. RSC Adv. **7**(11), 6323–6335 (2017)
27. Thaweesak, S., Lyu, M., Peerakiatkhajohn, P., Butburee, T., Luo, B., Chen, H., et al.: Two-dimensional g-C_3N_4/Ca_2N-b_2TaO_{10} nanosheet composites for efficient visible light photocatalytic hydrogen evolution. Appl. Catal. B **202**, 184–190 (2017)
28. Yang, F., Kuznietsov, V., Lublow, M., Merschjann, C., Steigert, A., Klaer, J., et al.: Solar hydrogen evolution using metal-free photocatalytic polymeric carbon nitride/$CuInS_2$ composites as photocathodes. J. Mater. Chem. A **1**(21), 6407–6415 (2013)
29. Wang, X., Maeda, K., Thomas, A., Takanabe, K., Xin, G., Carlsson, J.M., et al.: A metal-free polymeric photocatalyst for hydrogen production from water under visible light. Nat. Mater. **8**(1), 76–80 (2009)

30. Singh, V.K., Elomaa, O., Johansson, L.S., Hannula, S.P., Koskinen, J.: Lubricating properties of silica/graphene oxide composite powders. Carbon **79**, 227–235 (2014)

31. Kim, H.J., Kim, D.E.: Water lubrication of stainless steel using reduced graphene oxide coating. Sci. Rep. **5**, 17034 (2015)

32. Singh, V.K., Han, S.H., Yeon, J.R., Kim, J.H., Shin, K.: A simple green synthesis route for the reduction of graphene oxide and its application to Cu^{2+} removal. Sci. Adv. Mater. **5**(6), 566–574 (2013)

33. Chen, M., Kato, K., Adachi, K.: The difference in running-in period and friction coefficient between self-mated Si_3N_4 and SiC under water lubrication. Tribol. Lett. **11**(1), 23–28 (2001)

34. Xu, J.G., Kato, K., Hirayama, T.: The transition of wear mode during the running-in process of silicon nitride sliding in water. Wear **205**(1–2), 55–63 (1997)

35. Niu, Y., Zhao, J., Zhang, X., Wang, X., Wu, J., Li, Y., et al.: Large area orientation films based on graphene oxide self-assembly and low-temperature thermal reduction. Appl. Phys. Lett. **101**(18), 181903 (2012)

36. He, A., Huang, S., Yun, J.-H., Jiang, Z., Stokes, J., Jiao, S., et al.: The pH-dependent structural and tribological behaviour of aqueous graphene oxide suspensions. Tribol. Int. **116**, 460–469 (2017)

37. Zhang, L.L., Pu, J.B., Wang, L.P., Xue, Q.J.: Frictional dependence of graphene and carbon nanotube in diamond-like carbon/ionic liquids hybrid films in vacuum. Carbon **80**, 734–745 (2014)

38. Tomala, A., Karpinska, A., Werner, W., Olver, A., Störi, H.: Tribological properties of additives for water-based lubricants. Wear **269**, 804–810 (2010)

39. Bowden, F.P., Tabor, D.: Friction and Lubrication. Methuen, London (1960)

40. Liu, J.L., Feng, H.B., Wang, X.P., Qian, D., Jiang, J.B., Li, J.H., et al.: Self-assembly of nano/micro-structured Fe_3O_4 microspheres among 3D rGO/CNTs hierarchical networks with superior lithium storage performances. Nanotechnology **25**(22), 225401 (2014)

41. Zhang, L., Ni, Q.-Q., Fu, Y., Natsuki, T.: One-step preparation of water-soluble single-walled carbon nanotubes. Appl. Surf. Sci. **255**(15), 7095–7099 (2009)